



## Importance of soil thermal regime in terrestrial ecosystem carbon dynamics in the circumpolar north



Yueyang Jiang<sup>a,e</sup>, Qianlai Zhuang<sup>a,b,\*</sup>, Stephen Sitch<sup>c</sup>, Jonathan A. O'Donnell<sup>d</sup>, David Kicklighter<sup>e</sup>, Andrei Sokolov<sup>f</sup>, Jerry Melillo<sup>e</sup>

<sup>a</sup> Department of Earth, Atmospheric, and Planetary Sciences, Purdue University, West Lafayette, IN, USA

<sup>b</sup> Department of Agronomy, Purdue University, West Lafayette, IN, USA

<sup>c</sup> Geography, College of Life and Environmental Sciences, University of Exeter, Exeter, UK

<sup>d</sup> Arctic Network, National Park Service, Fairbanks, AK, USA

<sup>e</sup> The Ecosystems Center, Marine Biological Laboratory at Woods Hole, MA, USA

<sup>f</sup> Dept. of Earth, Atmospheric, and Planetary Sciences, Massachusetts Institute of Technology, Cambridge, MA, USA

### ARTICLE INFO

#### Article history:

Received 12 May 2014

Received in revised form 29 April 2016

Accepted 30 April 2016

Available online 03 May 2016

#### Keywords:

Soil thermal regime

Permafrost degradation

Active layer

Climate warming

Carbon budget

### ABSTRACT

In the circumpolar north (45–90°N), permafrost plays an important role in vegetation and carbon (C) dynamics. Permafrost thawing has been accelerated by the warming climate and exerts a positive feedback to climate through increasing soil C release to the atmosphere. To evaluate the influence of permafrost on C dynamics, changes in soil temperature profiles should be considered in global C models. This study incorporates a sophisticated soil thermal model (STM) into a dynamic global vegetation model (LPJ-DGVM) to improve simulations of changes in soil temperature profiles from the ground surface to 3 m depth, and its impacts on C pools and fluxes during the 20th and 21st centuries. With cooler simulated soil temperatures during the summer, LPJ-STM estimates  $-0.4 \text{ Pg C yr}^{-1}$  lower present-day heterotrophic respiration but  $\sim 0.5 \text{ Pg C yr}^{-1}$  higher net primary production than the original LPJ model resulting in an additional 0.8 to 1.0 Pg C  $\text{yr}^{-1}$  being sequestered in circumpolar ecosystems. Under a suite of projected warming scenarios, we show that the increasing active layer thickness results in the mobilization of permafrost C, which contributes to a more rapid increase in heterotrophic respiration in LPJ-STM compared to the stand-alone LPJ model. Except under the extreme warming conditions, increases in plant production due to warming and rising  $\text{CO}_2$ , overwhelm the enhanced ecosystem respiration so that both boreal forest and arctic tundra ecosystems remain a net C sink over the 21st century. This study highlights the importance of considering changes in the soil thermal regime when quantifying the C budget in the circumpolar north.

© 2016 Elsevier B.V. All rights reserved.

### 1. Introduction

Permafrost is an important control on vegetation and soil carbon (C) dynamics by affecting hydrological and soil thermal conditions in northern high-latitude ecosystems (Wania et al., 2009a; Schaphoff et al., 2013), which account for a large portion of the global C stocks (Hugelius et al., 2014). Recent climate warming has caused significant thawing of the near-surface permafrost across the circumpolar region (Romanovsky et al., 2015), including Alaska (Jorgenson et al., 2006; Osterkamp, 2007), Canada (Camill, 2005), and Russia (Streletskiy et al., 2015). Projected warming over the 21st century is expected to greatly reduce the areal extent of permafrost and seasonally frozen ground (Lawrence et al., 2012). If permafrost thaws, a fraction of soil organic C (SOC) in previously frozen layers will decompose and be

released as  $\text{CO}_2$  and  $\text{CH}_4$  (Olefeldt et al., 2012; Hayes et al., 2014; Johnston et al., 2014; Walter-Anthony et al., 2014). Furthermore, organic matter decomposition rates in unfrozen soils are sensitive to soil temperatures, which vary non-linearly across the soil column. Therefore, careful consideration of soil thermal regime changes (i.e. soil temperatures across the soil column from surface to deep soil layers) is important when simulating the potential future C loss from soils.

In addition to soil C, vegetation C pools are also sensitive to changes in soil thermal dynamics by permafrost thaw and rates of associated biogeochemical processes (Euskirchen et al., 2006). Field studies have indicated that permafrost thaw increases aboveground net primary production via increased nutrient availability (e.g., Schuur et al., 2007). While not explicitly testing the effects of thaw, other model studies have indicated a net C gain in circumpolar ecosystems because increased vegetation productivity more than compensated belowground C losses under a warming climate (Hartley et al., 2012; Koven, 2013). However, this net C gain may be optimistic as the effects of water stress and disturbances (e.g. insect infestations, wildfires) on permafrost-

\* Corresponding author.

E-mail addresses: [yueyang.jiang@oregonstate.edu](mailto:yueyang.jiang@oregonstate.edu) (Y. Jiang), [qzhuang@purdue.edu](mailto:qzhuang@purdue.edu) (Q. Zhuang).

region biomass are not adequately incorporated in current models (Abbott et al., 2016). Thus, large uncertainties currently exist regarding the magnitude and timing of this permafrost-C feedback to the climate system (Schoor et al., 2013), due in part to the complexity of ecosystem C processes in areas of degrading permafrost (e.g., thermokarst, thermal erosion) and their heterogeneity across regions.

To date, a number of studies have used process-based land surface models to estimate permafrost-C feedbacks under projected thaw scenarios (Koven et al., 2011; Harden et al., 2012; MacDougall et al., 2012; Schneider von Deimling et al., 2012). Soil thermal dynamics within these models vary in their complexity, from calculations of the cumulative active layer thickness distribution (e.g., Harden et al., 2012) to more sophisticated parameterizations of soil physics (e.g., MacDougall et al., 2012). Thaw dynamics are typically considered in a top-down one-dimensional manner, and heat transfer via conduction is the primary mode considered. However, the importance of soil water in non-conductive heat transfer (e.g., latent heat exchange, convection) has long been recognized as an important control on soil thermal dynamics (e.g., Romanovsky and Osterkamp, 2000). In this regard, our recent modeling studies that incorporate interactions between heat and water transport (Jiang et al., 2012a) have shown improvements in simulating the soil thermal regime changes in both tundra and boreal forest ecosystems in the northern high latitudes (Jiang et al., 2015).

To provide a better quantification of the ecosystem C budget in northern high latitudes and how this budget may change in the future, we use the Lund-Potsdam-Jena Dynamic Global Vegetation Model (LPJ-DGVM, Sitch et al., 2003; Gerten et al., 2004) coupled with a sophisticated soil thermal model (STM) by Jiang et al. (2012a) to conduct a set of simulations for both historical and future periods. The standard version of LPJ-DGVM has been widely used to simulate the global C budget and its response to climate change (e.g., Sitch et al., 2008; Jiang et al., 2012b). However, the model has used simplified soil temperature parameterizations for high-latitude regions (Sitch et al., 2003). Although later studies by Wania et al. (2009a, b) have taken steps to improve soil thermal and hydrologic parameterizations for permafrost conditions in northern peatlands, soil temperature and water dynamics are still modeled separately. As a consequence, the modeled active layer thickness exhibits poor agreement with observations (Wania et al., 2009b). Moreover, the effects of the vertical soil C distribution on decomposition have not been considered. In an extended LPJ, which includes managed land (LPJmL), Schaphoff et al. (2013) have recently coupled the interactions of soil water and heat transport, and considered vertically differentiated soil C stocks based on an organized soil C dataset in Jobbagy and Jackson (2000). However, the discrete vertical differentiation of the soil temperature profile in LPJmL is relatively coarse and the vertical distribution of SOC down to 3 m is highly concentrated in the uppermost soil layers (e.g., 0–20 cm) and does not consider long-term SOC accumulation in deep soil layers (Hugelius et al., 2014).

In this study, we integrate STM into LPJ to improve simulations of soil temperature dynamics from the ground surface to a depth of three meters, and the consequent impact on soil organic C stabilization and release across the northern permafrost region. Because the newly coupled version of the model, LPJ-STM, considers a fine vertical differentiation of soil temperatures, interactions of soil water with heat transport, and a vertical distribution of SOC with more C in deeper soil layers, we expect LPJ-STM to provide a more accurate quantification of the C budget for historical periods and to improve projections of carbon dynamics under future scenarios. To examine if LPJ-STM improved estimates of soil temperatures and associated carbon dynamics over LPJ, we compare estimates of both models to site observations of soil temperatures and net ecosystem production (NEP). In addition, simulated atmospheric carbon dioxide concentrations determined by using the model NEP estimates combined with an atmospheric transport model are compared to atmospheric flask measurements. To examine how improvements in simulated soil thermal regime affect the estimates of the contemporary C budget of northern high latitude ecosystems and its

projection into the 21st century, we compare estimates of net primary production (NPP), heterotrophic respiration ( $R_H$ ), and net ecosystem production (NEP) as well as vegetation and soil C stocks between LPJ and LPJ-STM.

## 2. Methods

### 2.1. Model description

The LPJ model simulates large-scale vegetation structure and land-atmosphere C and water fluxes in a modular framework (Sitch et al., 2003; Gerten et al., 2004). In the standard LPJ soil model, two soil layers have a fixed depth (i.e. 0.5 m and 1.0 m). The vertical distribution of soil C within these two soil layers is not explicitly considered. For permafrost thermal dynamics, LPJ calculates soil temperature at a depth of 25 cm in a very simplistic way based on the surface air temperature seasonal cycle with a dampened oscillation about a common mean and with a temporal lag (Sitch et al., 2003). The magnitude of the damping and temporal lag is related to soil texture, and the applied function assumes a sinusoidal variation in seasonal temperatures (Campbell and Norman, 1998). In this study, we replace the existing soil temperature scheme in the original LPJ with STM (Jiang et al., 2012a) to produce the coupled LPJ-STM model. Meanwhile, we modified the hydrology scheme following Wania et al. (2009b) and the representation of soil carbon dynamics following Schaphoff et al. (2013) in the LPJ-STM model.

#### 2.1.1. Soil thermal dynamics in LPJ-STM

While the original LPJ only includes a temperature calculation at a depth of 25 cm, LPJ-STM has a vertical differentiation of the soil temperature profile and provides a more complete depiction of soil thermal dynamics, including estimates of active layer thickness (ALT). Here, we estimate ALT using the 0 °C isotherm line as in Wania et al. (2009b). In LPJ-STM, the top three meters of soil is split into six layers with thicknesses of 10, 10, 10, 20, 50, and 200 cm (Fig. 1) that differ with respect to physical and hydraulic properties of boreal forest and tundra sites (Jiang et al., 2012a). These soil layer thicknesses are finer than the five soil layers used by Schaphoff et al. (2013) for the top 3 m: 20, 30, 50, 100, and 100 cm. In addition, unlike Schaphoff et al. (2013), LPJ-STM divides each of the soil layers into a number of depth-step increments to calculate soil temperatures. From the first to the sixth layer, the number of depth-step increments is respectively 10, 10, 10, 10, 20, and 40. To simulate perennially frozen ground, soil between 3 and 50 m is classified as the seventh layer with soil temperature simulated at 0.5 m depth-step increments.

Soil temperature is simulated numerically at each depth step by solving a modified Richards equation (Hansson et al., 2004; Saito et al., 2006). The governing equation for heat transport is as follows:

$$\begin{aligned} & \frac{\partial C_p T}{\partial t} - L_f \rho_i \frac{\partial \theta_i}{\partial t} + L_0(T) \frac{\partial \theta_v(T)}{\partial t} \\ & = \frac{\partial}{\partial z} \left[ \lambda \frac{\partial T}{\partial z} \right] - C_w \frac{\partial q_l T}{\partial z} - C_v \frac{\partial q_v T}{\partial z} - L_0(T) \frac{\partial q_v}{\partial z} - C_w S T \end{aligned} \quad (1)$$

where  $C_p$  ( $\text{J m}^{-3} \text{K}^{-1}$ ) is the volumetric heat capacity of the soil,  $C_w$  is the volumetric heat capacity of liquid water ( $4.18 \times 10^6 \text{ J m}^{-3} \text{K}^{-1}$ ),  $C_v$  is the volumetric heat capacity of water vapor ( $1.2 \times 10^3 \text{ J m}^{-3} \text{K}^{-1}$ ),  $\theta_i$  is the volumetric ice content (%),  $\theta_v$  is the volumetric unfrozen water content (%),  $t$  is time (units),  $z$  is depth (m),  $T$  is the absolute temperature (K),  $\rho_i$  is the density of ice ( $931 \text{ kg m}^{-3}$ ),  $L_0$  is the volumetric latent heat of vaporization of liquid water ( $\text{J m}^{-3}$ ),  $L_f$  is the latent heat of freezing ( $3.34 \times 10^5 \text{ J kg}^{-1}$ ),  $\lambda$  is the apparent thermal conductivity of soil ( $\text{J m}^{-1} \text{s}^{-1} \text{K}^{-1}$ ),  $q_l$  is the flux density of liquid water,  $q_v$  is the flux density of water vapor ( $\text{m s}^{-1}$ ), and  $S$  is a sink term accounting for root water uptake ( $\text{s}^{-1}$ ). While soil temperatures

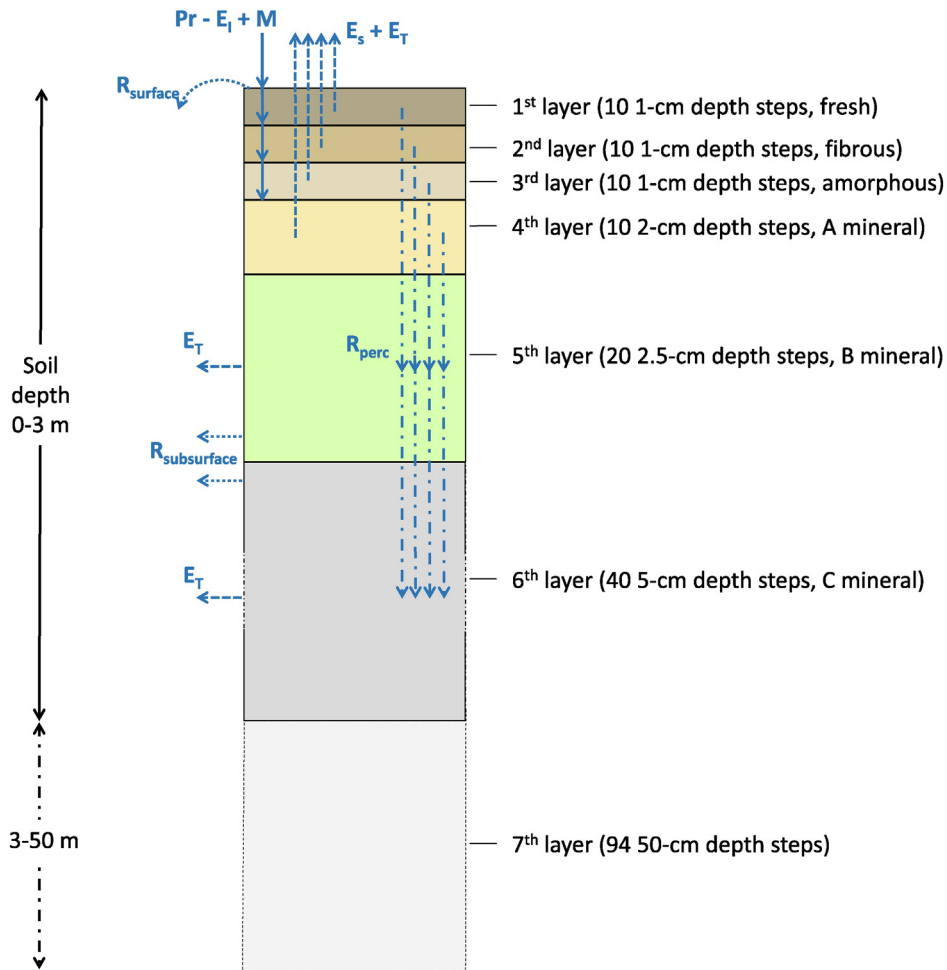


**Fig. 1.** Diagram illustrating hydrologic modeling framework in relation to soil profile structure. Vertical soil structure is divided into seven distinct layers (3 organic horizons, 3 mineral horizons and a deep horizon) that vary with respect to hydraulic properties ( $k$ , porosity, etc.). The model tracks and quantifies different water fluxes including precipitation ( $Pr$ ), interception by vegetation ( $E_i$ ); snow melt water ( $M$ ), evaporation ( $E_s$ ) transpiration ( $E_t$ ) runoff ( $R_{surface}$ ), subsurface flow ( $R_{subsurface}$ ), and percolation or infiltration ( $R_{perc}$ ). The solid arrows ( $\rightarrow$ ) reflect infiltration pathways of precipitation and snowmelt, which can be transferred from the ground surface to any of the top four layers. The dashed arrows ( $- \rightarrow$ ) reflect vertical water loss pathways via  $E_s$  and  $E_t$ , which can originate from the top three organic horizons or the uppermost mineral horizon. The dashed-dotted arrows ( $- \cdot \rightarrow$ ) reflect downward migration of soil water (i.e.  $R_{perc}$ ) which can occur across all soil horizons. The dotted arrows ( $\cdot \cdot \rightarrow$ ) indicate either pathways of  $R_{surface}$  at the ground surface, or  $R_{subsurface}$  from the B or C mineral horizons.

vary with depth step, the  $\theta_i$  and  $\theta_v$  used by LPJ-STM to calculate these temperatures (see below) are assumed to be uniformly distributed in each soil layer (i.e., do not vary with depth steps within a soil layer).

### 2.1.2. Hydrology in LPJ-STM

To match the layering scheme in STM, we simply modify the hydrology in LPJ partly following the routine in Wania et al. (2009b). The original top 0.5 m layer in LPJ now corresponds to the top four layers in LPJ-STM and the bottom layer (from 0.5 m to 1.5 m) in LPJ is extended to 3 m depth and corresponds to the fifth and sixth layer in LPJ-STM. The actual water holding capacity ( $AWHC$ , mm/mm) in each layer  $i$  is determined as the difference between the water hold capacity ( $WHC$ , mm/mm) and the ice content ( $icefr$ , mm/mm, estimated in STM):

$$AWHC_{(i)} = WHC_{(i)} - icefr_{(i)} \quad (2)$$

Of the top four layers (or top 50 cm, Fig. 1), the change in water content (mm) in each layer is determined as a layer-weighted difference of liquid water input (i.e. rainfall and melting water) and output (i.e. soil evaporation and transpiration), estimated in the LPJ hydrology module. In the top four layers, water in the  $i$ th layer exceeding  $AWHC_{(i)}$  is available for percolation into the 5th and 6th layers (Fig. 1). All these water fluxes (i.e., rainfall, melt water, soil evaporation, transpiration and

percolation) are estimated from the LPJ hydrology module (Gerten et al., 2004). In the 5th and 6th layer, the change in water content is calculated as the difference between percolation and transpiration. Within the 7th layer, the soil water content is assumed to be constant. The soil water content is updated daily in the hydrology routine, and then passed on to STM to calculate the soil temperature of each depth step in each layer. In the model, LPJ-STM does not consider hydraulic conductivity of water contents above field capacity. Roots can access water in the top six layers as long as the layer is not frozen.

### 2.1.3. Soil carbon dynamics in LPJ-STM

To provide a vertical distribution of the C pool across the soil column to 3 m deep (six layers, Fig. 1), we used a similar routine as that in Schaphoff et al. (2013):

$$SoilC_{total(i)} = d_{(i)}^K SoilC_{total} \quad (3)$$

where  $d$  (unitless) is the relative share of the  $i$ th layer in the entire soil pool and  $K$  (unitless) is the slope parameter that characterizes the relative rate of decrease with depth. In Schaphoff et al. (2013),  $K$  is varied by different plant functional types (PFTs) based on an optimized cumulative log-log equation from Jobbagy and Jackson (2000). Here, we use a

$K$  value of 0.7 for all PFTs to estimate SOC stock in each layer, based on the information of vertical soil C distribution in the recent databases (FAO/IIASA/ISRIC/ISSCAS/JRC, 2012; Hugelius et al., 2014).

Change in the total soil C stock,  $SoilC_{total}$  (g C/m<sup>2</sup>), is determined by the C input to soil from litter (i.e. 30% of decomposed litter goes into the soil C pool) and the C loss from soil by decomposition ( $k_{mean}$ ). The value of  $k_{mean}$  is determined as a layer weighted sum of the mean decomposition rate  $k_{mean(i)}$  in each soil C layer:

$$k_{mean} = \sum_{i=1}^{n_{layer}} (k_{mean(i)} \cdot d_{(i)}^K) \quad (4)$$

Within each soil layer, we calculate the decomposition rate of each depth step using the same soil temperature and moisture-dependent scheme as in Sitch et al. (2003). Then we determine  $k_{mean(i)}$  as the mean decomposition rate of all depth steps within the  $i$ th layer:

$$k_{mean(i)} = \frac{1}{n_{depthsteps}} \sum_{j=1}^{n_{depthsteps}} k_j \quad (5)$$

For example,  $k_{mean(i)}$  of the 1st layer is the mean of decomposition rates of all 10 depth steps (each step is 1 cm thick). This is different from Schaphoff et al. (2013), in which  $k_{mean(i)}$  is calculated using the mean soil temperature and soil moisture of layer  $i$ .

To mechanistically simulate the C shift between layers, following Schaphoff et al. (2013), the annual shift of C input  $C_{shift(i)}$  (unitless) for soil layer  $i$  into the lower layer due to cryoturbation and bioturbation is estimated by:

$$C_{shift(i)} = \frac{d_{(i)}^K k_{mean(i)}}{k_{mean}} \quad (6)$$

## 2.2. Climate forcing

In this study, monthly air temperature, cloud cover, precipitation, number of wet days, atmospheric CO<sub>2</sub> concentrations and soil property data are used to drive both LPJ and LPJ-STM. Historical climate data for 1901–2000 are obtained from the Climate Research Unit (CRU; Mitchell and Jones, 2005). The historical atmospheric CO<sub>2</sub> concentration datasets are from ice-core records and atmospheric observations (Keeling and Whorf, 2005), and soil texture data is derived from the FAO soil datasets (Zobler, 1986; FAO, 1991).

For the period 2001–2100, we use six climate scenarios produced with the MIT Integrated Global System Model (IGSM; Sokolov et al., 2005) under two emission scenarios (reference and level 1 stabilization cases) in the Synthesis and Assessment Product 2.1 of the U.S. Climate Change Science Program (Clarke et al., 2007; Webster et al., 2012). The reference emission scenario (REF), which assumes no climate policy, is very similar to the IPCC RCP8.5 scenario. The average CO<sub>2</sub> concentration over last decade of the 21st century in the IGSM REF simulations, with median settings for C cycle parameters and reference emission scenario, is 870 ppm (Sokolov et al., 2009; Webster et al., 2012), compared to 890 ppm from the IPCC RCP8.5 scenario. The corresponding total greenhouse gas forcing is an equivalent CO<sub>2</sub> concentration of 1330 and 1250 ppm, respectively. In contrast, the level 1 stabilization scenario (POL) assumes a rather stringent climate policy with global greenhouse gas emissions declining from year 2015 to year 2060 and staying fixed thereafter. As a result, CO<sub>2</sub> concentrations increase by the end of 21st century to only 480 ppm (560 ppm of CO<sub>2</sub>-equivalent), which falls in between the values for the IPCC RCP4.5 and RCP2.6. More detailed comparisons between the RCPs and the scenarios used in this study can be found in Webster et al. (2012).

Climate simulations for the two emission scenarios are carried out using three different sets of parameters defining the climate system

responses to anthropogenic emissions. These responses are dependent on climate sensitivity, the rate of heat uptake by the deep ocean, and the strength of aerosol forcing for a given emissions loading. Climate parameter sets corresponding to the 5th, 50th and 95th percentiles of the probability distribution for the increase in surface air temperature in the last decade of 21st century in the ensembles of simulations with REF and POL emissions (Sokolov et al., 2009) are chosen to represent low (L), median (M) and high (H) climate responses, respectively. The 90% probability ranges for the 21st century surface warming relative to 1981–2000 are 3.7–7.4 °C and 1.1–2.5 °C for the REF and POL scenarios respectively, with median values of 5.1 °C and 1.6 °C (Sokolov et al., 2009; Webster et al., 2012). Thus, the results from the six simulations used in this study (REF\_M, REF\_L, REF\_H and POL\_M, POL\_L, POL\_H) cover a very wide range of possible changes in future climate (Table 1).

## 2.3. Simulation protocols

Both the LPJ and LPJ-STM simulations are initially run for 2000 “spin-up” years before 1901, using a cyclic replication of climate data from 1901 to 1930. Similar to the strategy in Schaphoff et al. (2013), the first 990 years spin-up for LPJ-STM is run to achieve an equilibrium state of vegetation cover and mean-annual litter input into soils. The size of the slow soil C pool is analytically solved assuming a mean climate condition, and then we run for a further 1010 years with climate variability to initialize the soil C pool for each soil layer. From 1901 to 2100, the historical data (CRU, 1901–2000), followed by each of the six projected IGSM climates and CO<sub>2</sub> concentrations, are used to drive the simulations for the study region, which is represented by a total of 25,063 grid cells at a 0.5° latitude × 0.5° longitude resolution.

## 2.4. Evaluation of model performance

We compare the LPJ and LPJ-STM modeled soil temperatures with observations from eight sites studied in Jiang et al. (2012a) and compare the modeled soil water content with observation from three sites which have measurements at 25 cm soil. We also compare LPJ-STM modeled ALT with observations from 172 sites in GTN-P database (Biskaborn et al., 2015). To evaluate the model performance for simulating C dynamics, we first compare the simulated C fluxes from both LPJ and LPJ-STM to the measured NEP from FLUXNET sites (<http://fluxnet.ornl.gov>). For each FLUXNET site, the forcing data described in Section 2.2 for the grid cell containing the site is used to drive the model simulations for the comparisons. We acknowledge the uncertainty due to the mismatch of averaged grid cell climate and the site level climate, but we think this a common way to compare with site level observations. Moreover, at site level, the missing values of in-situ meteorological data can also lead to significant uncertainty if we use in-situ meteorological data to drive the model.

We also examine the ability of each model to reproduce seasonal fluctuations in atmospheric CO<sub>2</sub> concentration by using the modeled NEP across the circumpolar region to drive an atmospheric inversion and transport model, TM2 (Kaminski et al., 1999). The simulated CO<sub>2</sub> concentrations are then compared with the atmospheric flask

**Table 1**

Changes in annual mean air temperature ( $\Delta T_{air}$ ), annual total precipitation ( $\Delta PPT$ ), and atmospheric CO<sub>2</sub> concentration ( $\Delta CO_2$ ) between 2090s (2091–2100) and 2000s (2001–2010) in the six MIT IGSM climate scenarios used in this study (see text). All differences are calculated over the region ranging from 45°N to 90°N.

Scenario	$\Delta T_{air}$ (°C)	$\Delta PPT$ (mm)	$\Delta CO_2$ (ppmv)
POL_L	1.23	28.0	106
POL_M	1.70	40.5	93
POL_H	2.43	54.5	89
REF_L	5.01	94.5	530
REF_M	6.40	126.2	496
REF_H	8.42	162.4	488

measurements from monitoring stations. As in Heimann et al. (1998), we calculate the normalized mean-squared deviation (NMSD, equation is shown in Table 2) to evaluate the goodness of fit between the simulated and observed seasonal atmospheric CO<sub>2</sub> concentration.

### 3. Results

#### 3.1. Model performance

The LPJ-STM is able to well simulate the soil temperature profile for high latitude sites (Fig. 2). When compared with measured soil water content at 25 cm, LPJ-STM shows clearly better agreement than LPJ (Fig. 3). The LPJ-STM soil temperature estimates have lower root mean square error (RMSE) values than the LPJ estimates when compared against field measurements (Fig. 4). By replacing the LPJ soil temperature model with the STM, the seasonal temperature fluctuations are dampened with a much cooler soil during the growing season (the duration of the annual non-frozen period of the top 25 cm of soil) and a slightly warmer soil during the cold period (September–May). As shown in Jiang et al. (2012a), the soil temperature profile simulated by STM shows good agreement with observations at 11 sites, but the discrepancy between modeled and measured soil temperatures tends to increase with profile depth. Our model shows a clear latitudinal gradient of ALT in the circumpolar north (Fig. 5). Compared with ALT observations from 172 sites in GTN-P database (Biskaborn et al., 2015), a simple linear regression indicates a good agreement in general trends between modeled historical ALT and site observations (Fig. 5). However, the model tends to overestimate ALT at sites where the observed ALT is less than 100 cm and underestimate ALT at sites where the observed ALT is greater than 100 cm.

Compared with measured NEP at FLUXNET sites, LPJ-STM performs better than LPJ in reproducing monthly NEP (Fig. 6), based on more accurate simulation of NEP during the growing season. The larger amplitudes of the seasonal NEP cycles produced by LPJ-STM are mainly due to the lower summer R<sub>H</sub> and higher winter R<sub>H</sub>, relative to LPJ estimates.

When we use the NEP estimates from LPJ and LPJ-STM separately as inputs for TM2, and we find that the NEP from LPJ-STM leads to larger amplitudes of the seasonal cycles of CO<sub>2</sub>. This seasonal pattern is more

comparable with observations from not only the northern stations, but also stations in the tropics (30°N–30°S, e.g., Ascension Island) and Southern Hemisphere (30°S southward; e.g., Cape Grim, Tasmania), where the seasonal cycle is still largely influenced by atmospheric transport of CO<sub>2</sub> from the northern biosphere. Compared with NMSD values for models in Heimann et al. (1998), LPJ-STM performs better in reproducing the seasonal cycle of atmospheric CO<sub>2</sub> (Table 2).

#### 3.2. Changes in permafrost extent

The LPJ-STM projections indicate potential large changes in future soil thermal dynamics of circumpolar ecosystems. The model results show a substantial decrease in the extent of near-surface permafrost under the projected IGSM climates with the changes in extent being largely dependent on the warming strength (Fig. 7). Throughout the 21st century, the modeled decrease in permafrost extent varies among different climate scenarios, and the rate of permafrost loss increases during the second half of the century. In particular, under the REF\_H scenario, nearly 88% of near-surface permafrost (i.e. in top 3 m) will disappear by 2100, when there will be only relict permafrost at depths untied to prevailing climatic conditions (Fig. 7). Under the POL\_L scenario, only about 15% near-surface permafrost will disappear throughout the same time period. In general, the REF emission scenarios correspond to a larger loss of permafrost than the POL emission scenarios.

#### 3.3. Carbon budget

##### 3.3.1. Present-day

The two models achieve different initial equilibrium states in the year 1901, in which LPJ-STM estimates a smaller area covered by boreal deciduous forests than LPJ because LPJ-STM projects a shorter growing season and the photosynthesis of boreal deciduous trees is concentrated during the growing season. Instead, LPJ-STM estimates a larger area covered by evergreen forests than LPJ because the mid-summer NPP of boreal needleleaved trees is highly influenced by summer root respiration, which is lower in LPJ-STM because of the lower summer soil temperatures than that estimated with LPJ. Consequently, LPJ-STM estimates larger vegetation and soil C stocks (+13.7 Pg C or +8% and +430.2 Pg C or +50%, respectively, Table 3), and approximately 1.1 Pg C yr<sup>-1</sup> higher NEP than LPJ during the 1900s (Fig. 8).

Throughout the 20th century, LPJ-STM consistently yields ~0.5 Pg C yr<sup>-1</sup> higher NPP than LPJ, despite the shorter growing season. Compared with LPJ, the growing season length as simulated by LPJ-STM is 14 ± 8 days shorter at present, primarily due to later spring thaw (~10 ± 6 days), and to a lesser extent due to earlier refreezing in autumn (~4 ± 3 days). Unlike NPP, the difference in annual R<sub>H</sub> between LPJ-STM and LPJ gradually decreases from -0.6 Pg C yr<sup>-1</sup> in 1900s to around -0.4 Pg C yr<sup>-1</sup> for 2000s (Fig. 8). Larger NPP and smaller R<sub>H</sub> in LPJ-STM translates to 0.8–1.0 Pg C yr<sup>-1</sup> higher NEP in the 2010s, relative to those in LPJ. Spatially, almost the whole area underlain by permafrost (Fig. 5) exhibits stronger C sequestration in LPJ-STM relative to LPJ (Fig. 9). In particular, the strongest enhancement in annual NEP (+50 to +100 g C m<sup>-2</sup> yr<sup>-1</sup>) occurs in the Canadian boreal forest, Eastern Siberia and Mongolia, while the greatest reduction occurs in western Russia with up to a 90 g C m<sup>-2</sup> yr<sup>-1</sup> decrease in annual NEP.

The larger NPP in LPJ-STM maintains a higher vegetation C pool at present (i.e. 227.7–229.4 Pg), which is about 17.2–18.1 Pg C higher than in LPJ (i.e. 210.1–211.8 Pg, Table 3). Generally, the additional vegetation C estimated by LPJ-STM occurs mostly in boreal forest zones (e.g., the Alaskan and Canadian boreal forests) with up to 1.1 kg C m<sup>-2</sup> increases in vegetation C density (Fig. 9). Higher NPP also leads to more litter C input into the soil, and together with the lower R<sub>H</sub> contributes an ~430 Pg larger soil C pool in LPJ-STM during the 2010s (i.e. ~1297 Pg C, Table 3). The major differences in simulated soil C pool between the two models occur in the boreal forest eco-regions (e.g., the Alaskan, Canadian and Siberian boreal forests),

**Table 2**

Normalized Mean Squared Deviation (NMSD) between simulated and observed seasonal cycle of CO<sub>2</sub>; for comparison of the observed with the TM2 simulated seasonal cycles of CO<sub>2</sub>, produced by coupling the monthly net ecosystem productivity by LPJ and LPJ-STM for northern, tropical and southern monitoring stations. The station data is from Heimann et al. (1998), for the period of 1983–1992.

Station	Coordinate	LPJ	LPJ-STM	Average <sup>a</sup>
Alert, Northwest Territories	82°27'N, 62°31'W	17.8	14.3	28.4
Point Barrow, Alaska	71°19'N, 156°36'W	12.3	11.5	13.2
Cold Bay, Alaska	55°12'N, 162°43'W	10.5	5.8	11.1
Cape Meares, Oregon	45°29'N, 124°00'W	6.7	4.3	18.6
Azores (Terceira Island)	38°45'N, 27°05'W	1.7	1.1	4.0
Niwot Ridge, Colorado	40°03'N, 105°38'W	6.1	3.0	5.9
Sand Island, Midway	28°13'N, 177°22'W	9.4	4.5	8.8
Key Biscayne, Florida	24°40'N, 80°12'W	6.4	3.7	9.7
Cape Kumukahi, Hawaii	19°31'N, 154°49'W	29.4	16.8	14.7
St. Croix, Virgin Islands	17°45'N, 64°45'W	9.2	6.3	6.2
Seychelles (Mahe Island)	4°40'S, 55°10'E	2.2	1.9	1.0
Ascension Island	7°55'S, 14°25'W	4.3	4.1	10.6
American Samoa	14°15'S, 170°34'W	1.3	1.4	5.2
Cape Grim, Tasmania	40°41'S, 144°41'E	1.6	1.1	17.4
Amundsen Scott (South Pole)	89°59'S, 24°48'W	6.5	5.8	34.7

$$NMSD = \frac{1}{12} \sum_{m=1}^{12} \left( \frac{C_{T,m} + C_{F,m} + C_{O,m} - C_{OBS,m}}{\sigma_m} \right)^2$$
 NMSD is calculated as the normalized square of difference between the sum of monthly CO<sub>2</sub> concentration from biospheric (C<sub>T,m</sub>), fossil fuel (C<sub>F,m</sub>), ocean flux (C<sub>O,m</sub>), and the 10-year mean of observed CO<sub>2</sub> flux values (C<sub>OBS,m</sub>) for the period 1983–1992. The factor used to normalized the difference is the standard deviation (σ<sub>m</sub>) of the observed value for each month (m = 1, ..., 12) of the year.

<sup>a</sup> The mean value of NMSDs from five prognostic models (BIOME2, FBM, SILVAN, and TEM) used in Heimann et al. (1998).

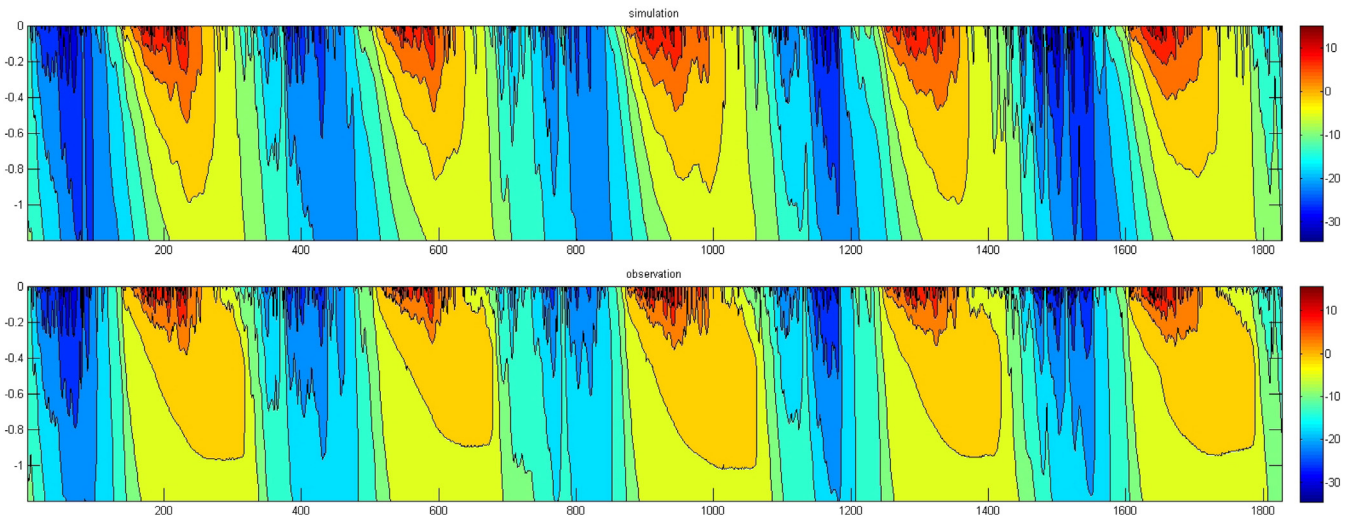


Fig. 2. LPJ-STM simulated (top) and observed (bottom) soil temperature profile at the Westdock site (using probe 2 data).

where LPJ-STM produces up to  $20 \text{ kg C m}^{-2}$  higher soil C stocks (Fig. 9). The LPJ-STM simulations indicate that the continuous permafrost in the far northern regions and Mongolia store the largest soil C pools in the circumpolar north.

LPJ-STM does better than LPJ in simulating the SOC pool when compared with two major global soil C datasets. In particular, LPJ-STM estimates higher soil C than the land-based Harmonized World Soil Database (HWSD, FAO/IIASA/ISRIC/ISSCAS/JRC, 2012), but lower soil C in permafrost areas ( $\sim 17.8 \times 10^6 \text{ km}^2$ , Fig. 10) defined by the Northern Circumpolar Soil Carbon Database version 2 (NCSCDV2, Tarnocai et al., 2009; Hugelius et al., 2014). In particular, LPJ-STM estimates  $177 \text{ Pg C}$  for the top 30 cm of the soil profile compared to  $151 \text{ Pg C}$  by HWSD and  $217 \pm 12 \text{ Pg C}$  by NCSCDV2. For the top 100 cm of the soil profile, LPJ-STM estimates  $389 \text{ Pg C}$  compared to  $288 \text{ Pg C}$  by HWSD and  $472 \pm \text{ Pg C}$  by NCSCDV2. The higher SOC stocks estimated by LPJ-STM relative to HWSD occur in most areas underlain by permafrost (e.g., Siberia, Alaska, and Canadian boreal forest and tundra, Fig. 10). The lower SOC stocks estimated by LPJ-STM relative to NCSCDV2 mainly occur in Siberia.

### 3.3.2. Future carbon budgets

Under the warming scenarios, both models predict significant increases in annual NPP and  $R_H$ , where the magnitude is largely controlled by the severity of climate change (Table 4). In particular, the reference climate scenarios cause an approximate increase of 47–59% in annual NPP by 2100, but only  $\sim 10\%$  accrual under the policy climate scenarios (Table 4). In parallel, the NPP difference between LPJ-STM and LPJ increases from around  $0.5 \text{ Pg C yr}^{-1}$  to  $0.8\text{--}0.9 \text{ Pg C yr}^{-1}$  under the reference scenarios, but exhibits only a slight increase ( $\sim 0.1 \text{ Pg C yr}^{-1}$ ) under

the policy scenarios (Fig. 8). Changes in  $R_H$  show similar patterns of response to the climate variability as those of NPP (Table 4), while the difference in  $R_H$  between the two models shows a clear decreasing trend through all six warming scenarios (Fig. 8).

As the difference of NPP and  $R_H$ , the NEP in both models is simulated to decrease over the 21st century, because the annual  $R_H$  increases faster than NPP, especially under the severe warming scenarios (Table 4). For example, forced by the REF\_M and REF\_H scenarios, the study region eventually shifts from a C sink to a source by 2090s. Meanwhile, the NEP difference between the two models exhibits a clear decline (from  $\sim 0.9$  to  $\sim 0.6 \text{ Pg C yr}^{-1}$ ) through the 21st century, despite the strong inter-annual variability (Fig. 8). However, the significant positive difference here indicates that the introduction of STM into LPJ contributes to maintaining the modeled capacity of C sequestration in the circumpolar north.

Given the enhanced plant productivity associated with warming and  $\text{CO}_2$  increase, both models predict a large increase in the vegetation C pool, which is  $18.4\text{--}22.3 \text{ Pg C}$  larger in LPJ-STM ( $294.1\text{--}358.0 \text{ Pg C}$ ) than in LPJ ( $275.7\text{--}336.4 \text{ Pg C}$ ) by 2090s (Table 3). Driven by six warming scenarios, LPJ projects substantive soil C loss ( $-26.5$  to  $-58.8 \text{ Pg C}$ ), and LPJ-STM projects a  $2.8\text{--}34.1 \text{ Pg C}$  gain in soil C stock over the period of 2000–2100 under four out of the six IGSM climates but  $5.3$  and  $27.1 \text{ Pg C}$  soil C loss under REF\_M and REF\_H (Table 3).

## 4. Discussion

In this study, we examine how a more detailed representation of soil thermal dynamics, soil hydrology, and soil C dynamics influences estimates of C fluxes and pools of ecosystems in the circumpolar north.

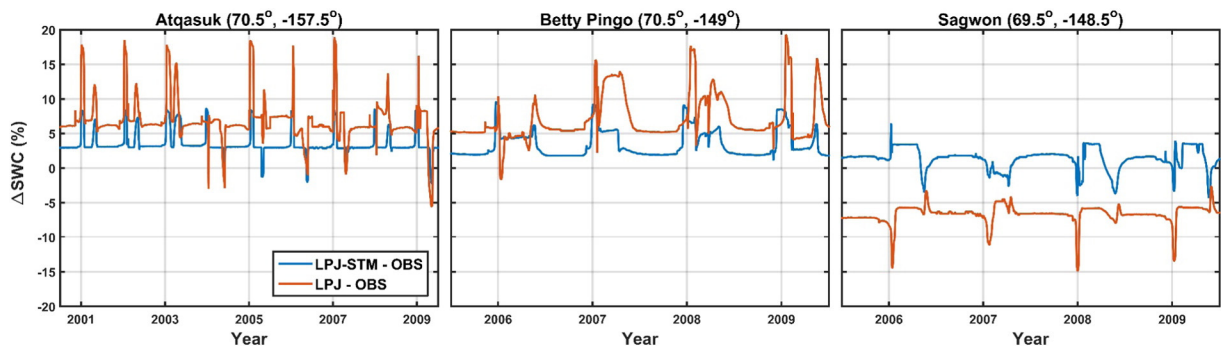
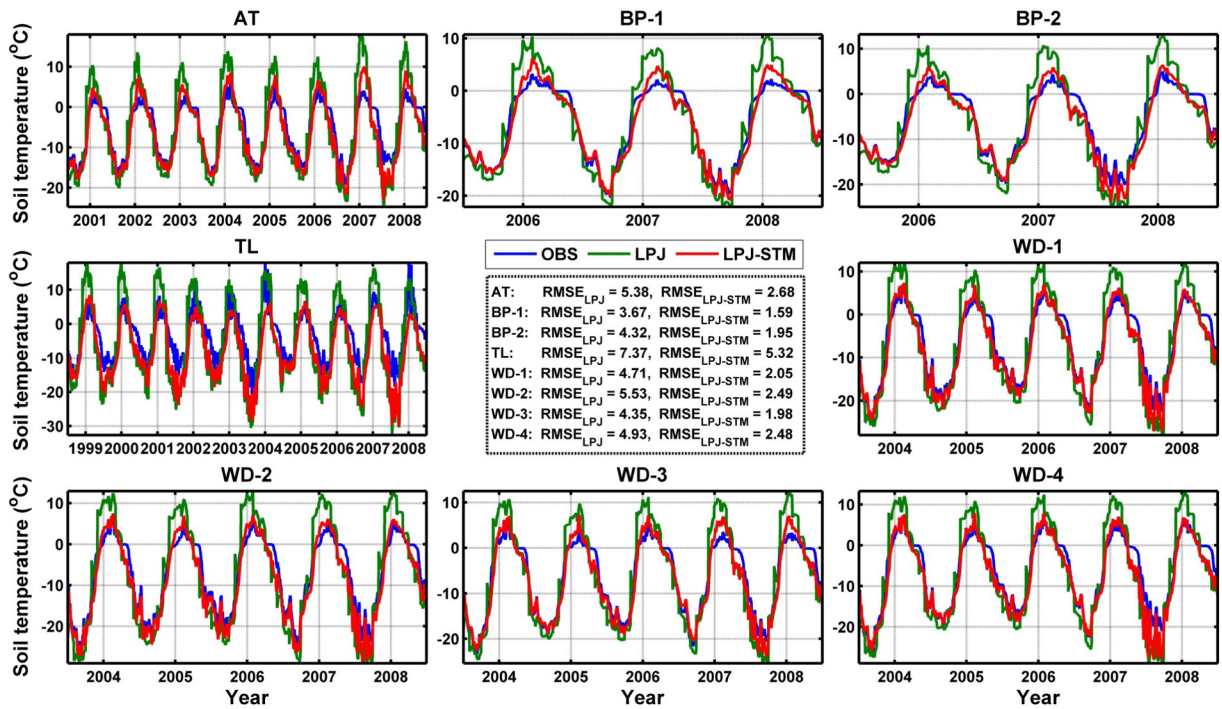


Fig. 3. Difference in soil moisture at 25 cm by LPJ and LPJ-STM relative to observations at three sites.



**Fig. 4.** Observed and simulated daily soil temperature at 25 cm with STM and the soil temperature algorithm in LPJ at eight sites. RMSE represents the root mean square error from the fit between observations and simulations. AT: Atkasuk ( $70.5^{\circ}$ ,  $-157.5^{\circ}$ ); BP: Betty Pingo ( $70.5^{\circ}$ ,  $-149^{\circ}$ ); TL: Toolik ( $68.5^{\circ}$ ,  $-149.5^{\circ}$ ); WD: Westdock ( $70.5^{\circ}$ ,  $-148.5^{\circ}$ ). BP-1 and BP-2 are two different sites, and WD-1, 2, 3, 4 are four different sites.

The detailed representation of these ecosystem processes in LPJ-STM estimates higher NPP, but lower RH for current circumpolar ecosystems than the more aggregated representation of these processes in LPJ. As a result, more C ( $0.8$  to  $1.0$  Pg C yr $^{-1}$ ) is estimated to be sequestered in these ecosystems by LPJ-STM with almost all of the additional C (96%) being stored in soils. With global warming, the LPJ-STM still estimates more C is sequestered in the future than LPJ with most of the additional C being stored in soils, but the difference between model estimates decrease over time. Below we focus our discussion on: 1) how the LPJ-STM improved the quantification of present-day C budgets; 2) how these improvements affect projections of future permafrost degradation and their effects on C dynamics; and 3) sources of uncertainty in simulating C dynamics in the circumpolar north region.

#### 4.1. Present-day soil C budgets

The increase in annual  $R_H$  as simulated in both models is mainly driven by the warming soil temperatures. The addition of vertical differentiation of the soil temperature profile and a depth distribution of soil C in LPJ-STM improves the representation of soil physical and biogeochemical processes. This leads to a more accurate simulation of thawing and refreezing processes as well as ALT estimates, further reducing the model errors in soil C stock. The lower summer soil temperatures produced by LPJ-STM largely stabilize soil C by reducing  $R_H$ , especially for the top layers (e.g., the upper 30 cm, Fig. 10). The impact of considering permafrost on  $R_H$  in our simulation is different from Wania et al. (2009a), who shows that the introduction of permafrost increases soil

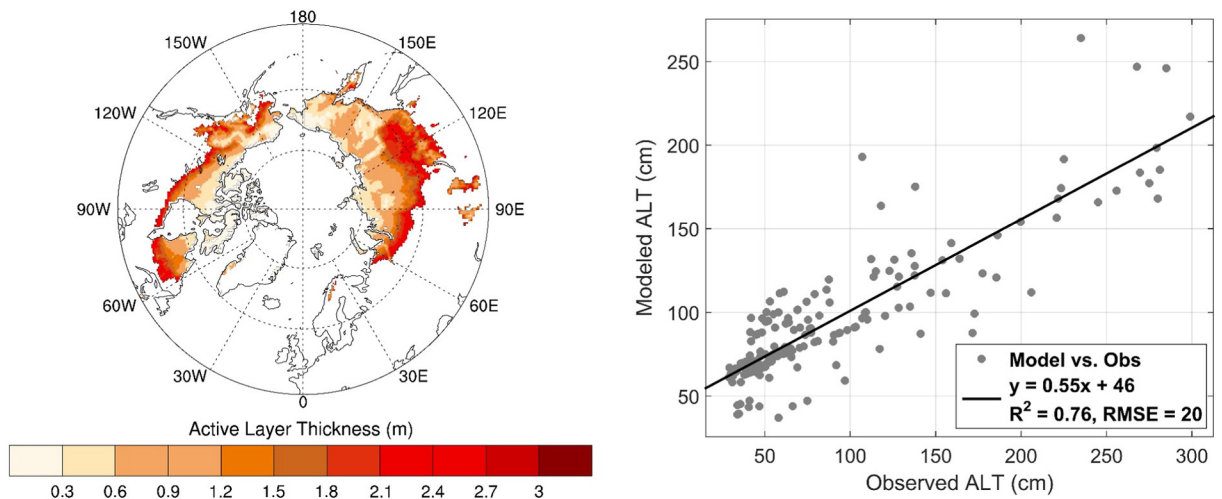


**Fig. 5.** Modeled distribution of active layer thickness (ALT) in areas underlain by permafrost in 2000 (left) and a comparison (right) between modeled and observed ALT at 172 sites derived from the GTN-P database (Biskaborn et al., 2015). The dash line represents the 1:1 line.

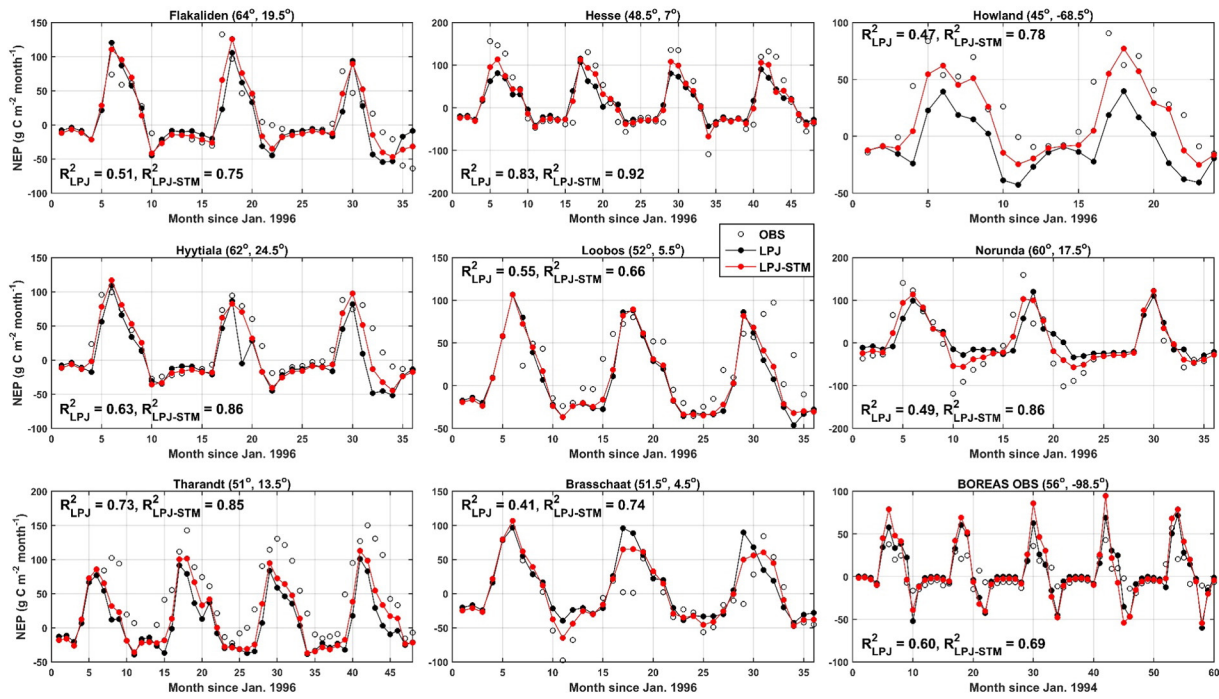


**Fig. 6.** Observed and simulated monthly NEP ( $\text{g C m}^{-2}$ , positive value means a C flux to the biosphere, and negative value represents a C flux to the atmosphere) with LPJ and LPJ-STM at nine sites (latitude and longitude shown in parentheses) located north of latitude  $45^\circ\text{N}$ .  $R^2$  represents the coefficient of determination from simple linear regressions. Observed NEP data were obtained via the FLUXNET database (<http://fluxnet.ornl.gov>).

respiration by about  $0.39 \text{ Pg C yr}^{-1}$  probably because LPH-Why simulates higher soil C stock ( $+39 \text{ Pg C}$ ) over 1991–2000. However, LPJ-STM estimates lower ( $-0.6 \text{ Pg C yr}^{-1}$ )  $R_H$  than LPJ mainly because LPJ-STM estimates significantly lower summer soil temperatures than LPJ, even though LPJ-STM has a larger soil C pool than LPJ. As demonstrated in Schaphoff et al. (2013), saturated hydraulic conductivity may also play an important role in the C balance, as  $R_H$  achieves peak rates around field capacity and decreases as water saturation is approached because of decreasing soil oxygen content. Because we did not consider water contents above field capacity in our analyses,  $R_H$  may be somewhat overestimated in our study. In addition,  $R_H$  may also be overestimated at sites where the model overestimates the size

of the active layer (Fig. 5). Consequently, our estimates of soil C pool in the circumpolar north may be conservative, especially in regions with high water content (e.g., wetland).

The slightly lower SOC from LPJ-STM relative to NCSCDv2 is probably due to not considering the effects of some important processes in our model that influence deep C storage in the northern permafrost region, such as peatland development (Smith et al., 2014; Treat et al., 2016), syngenetic permafrost aggradation in areas of loess deposition (i.e. Yedoma; Shur et al. 2004), and alluvial deposition (i.e. large river deltas; Hugelius et al., 2014). Northern peatlands in particular store large amounts of SOC, with approximately 184 and 94  $\text{Pg C}$  in Histels (i.e. permafrost peatlands) and Histosols (non-permafrost peatlands), respectively (Tarnocai et al., 2009; Yu et al., 2010). Moreover, the model-data differences could be partly attributed to the spatial heterogeneity caused by disturbances that have not been explicitly simulated in the model, such as fire and thermokarst (Grosse et al., 2011). Similar to our results, lower estimates of SOC relative to NCSCDv2 have been observed in other earth system models (Todd-Brown et al., 2013). Compared with HWSD, LPJ-STM estimates higher SOC stocks in most of the permafrost affected areas. It is difficult to evaluate these differences, however, because HWSD has not included enough information about how their estimates were derived.

We estimate that approximately 844  $\text{Pg C}$  are stored within the top 3 m of soils, which is slightly lower than the estimates of  $1035 \pm 150 \text{ Pg C}$  in Hugelius et al. (2014). We recognized that, in parts of the circumpolar north, soils might not extend to a depth of 3 m or even be present in areas with bedrock near or at the surface. In other areas, there is widespread occurrence of massive ground ice (Schirrmeister et al., 2011) as in regions with deep yedoma deposits (Kanevskiy et al., 2011). Because these factors are not accounted for in LPJ-STM, our model may overestimate the SOC stocks in the region. Meanwhile, some important soil forming processes (e.g., peat formation, cryoturbation) that greatly influence the distribution of SOC in deep soil layers (Bockheim, 2007; Hugelius et al., 2010) are not mechanistically modeled, which may cause bias in SOC estimates, especially in the mineral soil layers. Therefore, in ice-rich permafrost areas, model-data differences in deep layer SOC can be substantial. However, due to

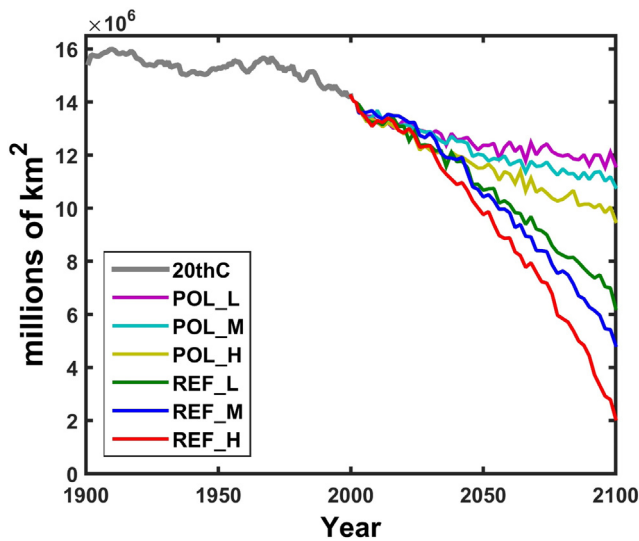


**Fig. 7.** Time series of near surface permafrost extent in the  $45^\circ\text{N}$  northward region simulated with LPJ-STM for the historical and projection periods. Near-surface permafrost extent is the integrated area of  $0.5^\circ \times 0.5^\circ$  grid cells with the maximum active layer shallower than 3 m.

**Table 3**  
The average carbon stocks in the 1900s, 2010s and 2090s estimated with LPJ and LPJ-STM.

	Vegetation carbon (Pg C)						Soil carbon (Pg C)					
	LPJ			LPJ-STM			LPJ			LPJ-STM		
	1900s	2010s	2090s	1900s	2010s	2090s	1900s	2010s	2090s	1900s	2010s	2090s
Historical	165.0	–	–	178.7	–	–	867.1	–	–	1297.3	–	–
POL_L	–	210.7	336.4	–	228.8	358.0	–	864.1	837.6	–	1319.4	1350.8
POL_M	–	210.2	326.3	–	227.8	347.6	–	864.0	833.4	–	1319.3	1335.6
POL_H	–	211.7	334.1	–	228.9	355.7	–	864.0	825.4	–	1319.3	1322.1
REF_L	–	210.6	333.4	–	228.0	355.7	–	863.9	827.1	–	1319.5	1335.6
REF_M	–	210.1	316.3	–	227.7	337.3	–	864.1	818.6	–	1319.7	1314.4
REF_H	–	211.8	275.7	–	229.4	294.1	–	864.0	805.2	–	1319.3	1292.2

Note that the top 3 m soil C stock in LPJ-STM were used to compare with the soil C pool modeled with LPJ, which does not explicitly model soil carbon at different depths.

the scarce field data (i.e. few sampled pedons) and limited quantification of spatial variability in both ground ice content and soils, the empirical SOC data in some remote areas (Mishra et al., 2013), and in regions of thin sedimentary overburden (e.g., highlands and alpine terrain) have relatively high uncertainty (Hugelius et al., 2014). Therefore, more field measurements in deep soil layers and representation of spatial distribution of shallow soils and ground ice are needed to better constrain the regional simulations of SOC in the permafrost zone.

LPJ-STM produces lower  $R_H$  than LPJ mainly because of the lower summer soil temperatures in the active layer and the freezing conditions below, where microbial activity is limited. The higher NPP in LPJ-STM is a counter-balance between the reduced summer below-ground autotrophic respiration due to cooler soil temperature, and the decrease in water availability associated with the decreased rooting depth in permafrost affected areas. The enhancement in  $CO_2$  exchange through amplified plant productivity in LPJ-STM is consistent with the finding in Forkel et al. (2016). However, our simulation results are different from Wania et al. (2009a), who show that integrating a simple permafrost model into LPJ slightly reduced circumpolar (45–90°N) NEP due to the decrease in NPP and increase in  $R_H$ .

#### 4.2. Permafrost degradation and its implications for future carbon budget

Compared with the simulated permafrost extent in Lawrence et al. (2012), our study estimates a slightly larger extent of the entire permafrost zone in the early 2000s. Driven by the range of MIT IGSM climate scenarios, we estimate large variabilities in permafrost extent by 2100 (Fig. 7), which are comparable to the projections in Slater and Lawrence (2013). The lower boundary of modeled permafrost retreat (i.e. ~23% reduction in permafrost area under the coolest climate, POL\_L), is similar to the estimate in a conservative permafrost model (Anisimov and Reneva, 2006) that predicts an approximate 19–24% reduction in near-surface permafrost area by 2080. At the biome level, our simulated range of permafrost degradation also covered the range of estimates from other model simulations (e.g., Stendel and Christensen,

2002; Zhang et al., 2008). For example, our projected permafrost extent under the IGSM policy scenarios in the Canadian boreal forest region is similar to Zhang et al. (2008) who show a 15–19% reduction in the extent of permafrost through the 21st century. Although the rate of permafrost retreat could potentially be faster than the migration of boreal deciduous forests, the presence of permafrost still constrains the northward expansion of boreal broadleaved summergreen trees, which is consistent with the findings in Tchebakova et al. (2009). As the southern boundary of permafrost moves northward, temperate forests are projected to migrate to the north and gradually replace the boreal forests. This expansion is partly because temperate trees are favored in the warming climate by our model.

The reduced difference in future NEP between LPJ-STM and LPJ (Fig. 8) occur for a number of reasons. The more positive effect of permafrost on the C sink by LPJ-STM compared to LPJ will decrease as the permafrost degrades because more of the newly thawed labile SOC pool will be exposed to decomposition in LPJ-STM. The projected replacement of boreal evergreen conifer forests with herbaceous and deciduous vegetation in the thawing permafrost area can influence the C inputs to mineral soil, because of variations in productivity among these biomes (Jobbagy and Jackson, 2000) and in the ability of roots to access the mineral substrate (O'Donnell et al., 2011). As permafrost thaws, areas with a transition from boreal evergreen forest to temperate deciduous forest exhibit a fast decline in annual NEP, although the NPP increases rapidly due to a larger temperature range for temperate types (Sitch et al., 2008). This implies that the enhancement in biomass productivity by vegetation change in the boreal zone could not offset the C loss through increased  $R_H$  by warming climate. Because both models predict a declining trend in annual NEP, the reduced model difference implies a faster reduction in NEP by LPJ-STM. This indicates a high sensitivity of C sequestration to permafrost degradation, especially under severe warming scenarios (e.g., REF\_H).

Unlike LPJ that projects a reduced SOC pool throughout the 21st century because of the warming-stimulated SOC decomposition, LPJ-STM predicts a gain in the SOC pool over this century except the REF\_M

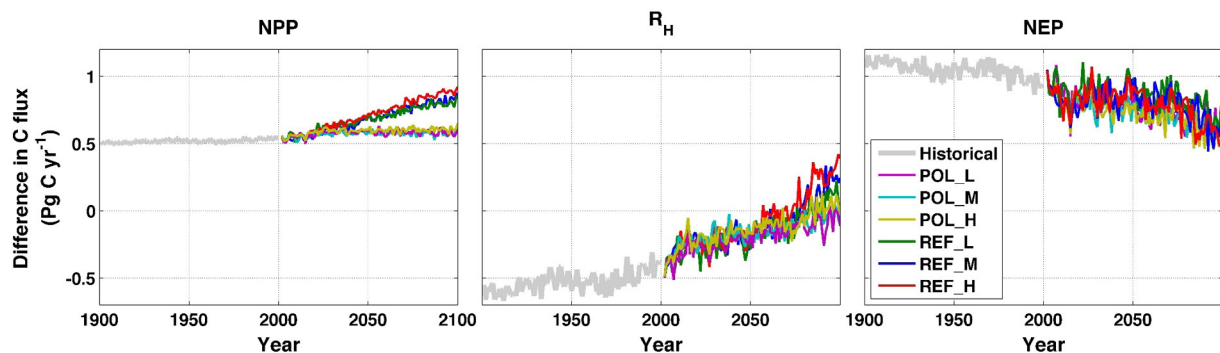


**Fig. 8.** Difference (LPJ-STM minus LPJ) in modeled annual net primary production (NPP), heterotrophic respiration ( $R_H$ ) and net ecosystem productivity (NEP) of the circumpolar north for the historical period and six future projections.

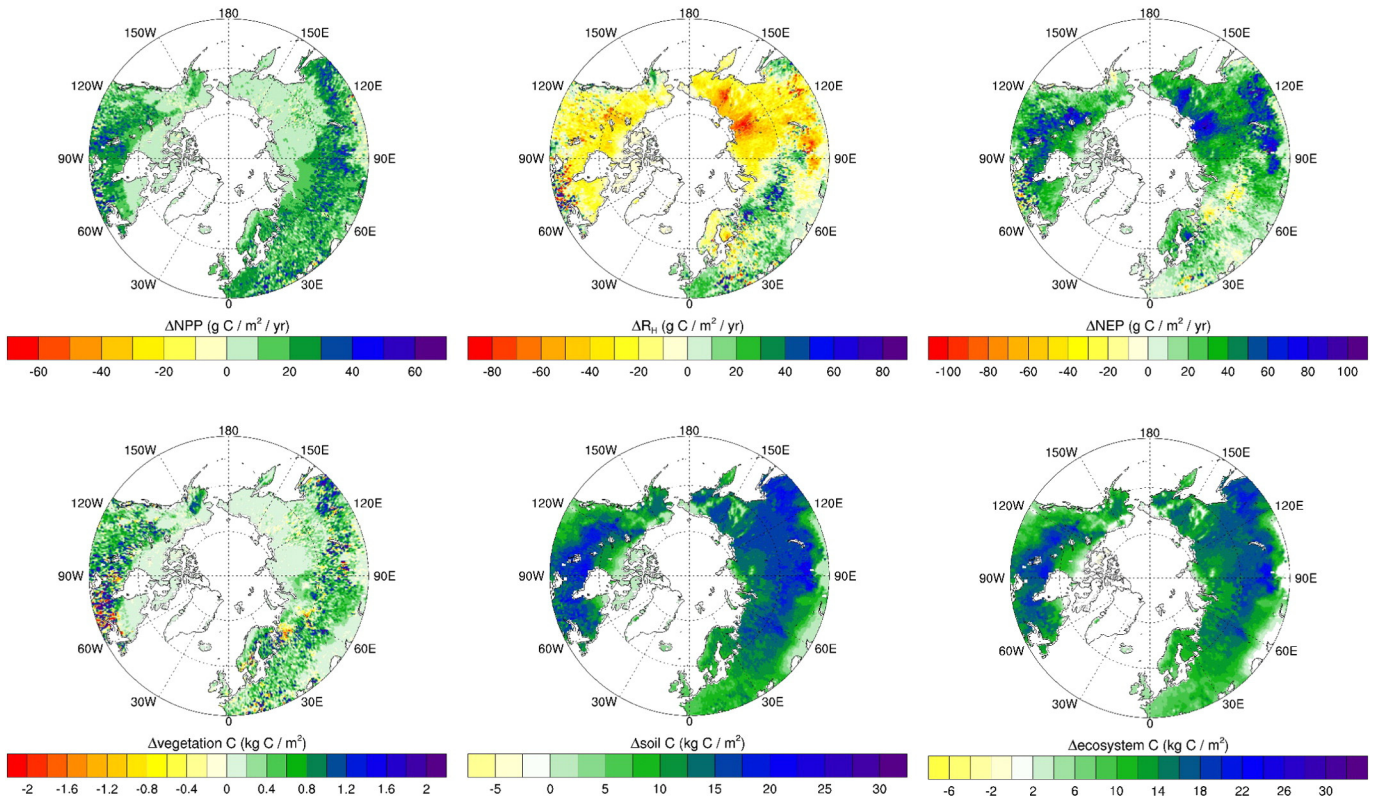


**Fig. 9.** Distribution of the differences (LPJ-STM minus LPJ) of modeled mean annual carbon fluxes ( $\Delta$ NEP,  $\Delta$ RH,  $\Delta$ NEP) and mean carbon standing stocks ( $\Delta$ vegetation C,  $\Delta$ soil C,  $\Delta$ ecosystem C stocks) during the 2000s for the circumpolar region north of 45°N.

and REF\_H scenarios (Table 3). In LPJ-STM, increased litter C inputs from the stimulated plant growth are sufficient to compensate for the loss of SOC by decomposition, which is greatly suppressed by the simulated cooler summer soil temperature. However, we also notice that as soil temperature increases, litter decomposition becomes stronger and the amount of decomposed litter turning into SOC becomes insufficient to compensate for the respiratory C loss from soil. As a result, SOC accumulation slows down and even declines during the second half century under severe warming scenarios (e.g., REF\_H).

4.3. Sources of uncertainty

Despite the improved simulation of soil temperatures, LPJ-STM still likely overestimates NPP because nitrogen limitations to NPP have not been explicitly considered as in other modeling studies (Sokolov et al., 2008; Xu and Prentice, 2008; Smith et al., 2014) or shown in field studies (Nordin et al., 2004; Hobara et al., 2006). However, increased nitrogen mineralization associated with enhanced decomposition from permafrost degradation (Keuper et al., 2012; Koch et al., 2013, 2014; Hayes et al., 2014; Walter-Anthony et al., 2014) may cause nitrogen to be more available to NPP in permafrost environments than in other biomes under warming conditions, especially in well-drained tundra ecosystems with deep rooting zones (Shaver et al., 2001; Mack et al., 2004; Schuur et al., 2007).

Permafrost degradation can also cause a substantial change in surface hydrology, which will further influence the vegetation dynamics and C balance in the region. For example, in ice-rich and poorly-drained permafrost areas, permafrost degradation will cause substantial ground-surface subsidence and ponding where the over-saturated conditions may increase tree mortality in boreal forests (Osterkamp et al., 2000; Jorgenson et al., 2001). Long-term permafrost degradation will eventually promote subsurface water drainage and increase the dryness

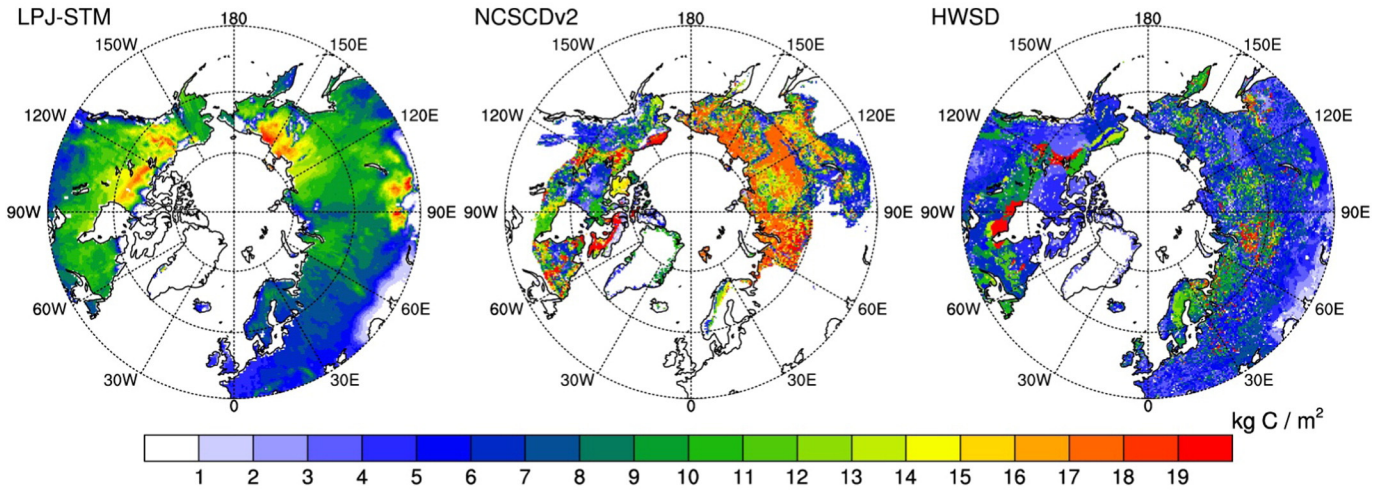
of soils (Yoshikawa and Hinzman, 2003). In peatlands, the warming-caused declines in water table may increase soil decomposition, leading to a long-term C loss (Oechel et al., 1998; Ise et al., 2008; Sulman et al., 2009; Olivas et al., 2010). In contrast, a low water table may cause a long-term C gain in non-peat wetlands (Sulman et al., 2010). Given the importance of hydrological change on C balance, future C models should be coupled with climate-driven hydrological models (e.g., Wania et al., 2009a,b).

Another uncertainty source is fire disturbance. Future stimulated fire regimes in both boreal forest (Turetsky et al., 2010), and tundra landscapes (Rocha et al., 2012) will exacerbate the permafrost degradation rate relative to the change from warming alone (Lawrence et al., 2012; Schuur et al., 2013; Jiang et al., 2015). Fires may therefore play a more important role in C dynamics of the circumpolar north. However, the fire-caused change in permafrost thaw has not been accounted in current modeling work. A more mechanistic description for the relationships between fire, permafrost and C dynamics is necessary for future modeling efforts.

5. Conclusions

This study examines the importance of changes in the soil thermal regime on determining the C budget in the circumpolar north. With explicitly modeled temperatures at different depths, the LPJ-STM model estimates larger soil organic C stocks in the circumpolar north, which agrees well with empirical global data sources. Our model simulations indicate that, although most biogeochemical processes of C storage and decomposition take place in top soil layers (i.e. top 30 cm), deep layers also substantially influence the SOC dynamics, especially when these layers confront a phase change. Some missing processes that affect the soil thermal regimes (e.g., formation of taliks, absence of snow dynamics) still result in a significant uncertainty of our estimates.

(a)



(b)

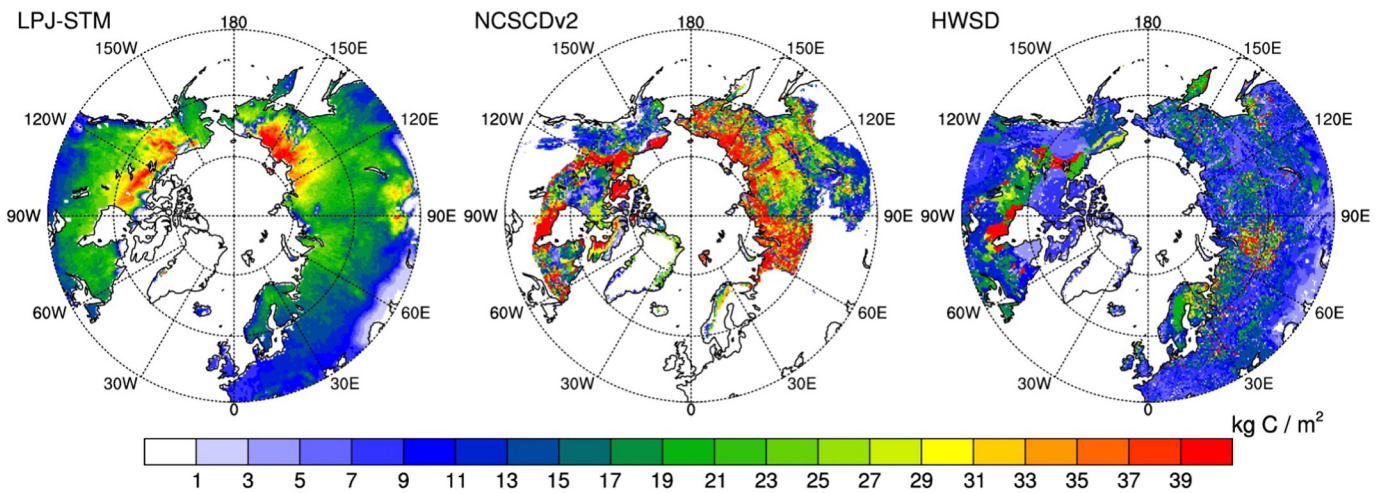


**Fig. 10.** Carbon density ( $\text{kg C m}^{-2}$ ) in the top 30 cm (a) and 100 cm (b) of soil estimated by LPJ-STM for the year 2000, the Northern Circumpolar Soil Carbon Database version 2 (NCSCDv2, Hugelius et al., 2014), and the Harmonized World Soil Database (HWSD, FAO/IIASA/ISRIC/ISSCAS/JRC, 2012).

Thus more field measurements of deep soil organic carbon are needed. This study highlights the importance of a more adequate representation of soil thermal dynamics in dynamic global vegetation models, such as LPJ, for quantifying C responses to climate change in northern high latitudes.

#### Acknowledgment

We thank Jessica Drysdale for comments on earlier drafts of this manuscript. This research is supported by funded projects to Q. Z. National Science Foundation (NSF-1028291 and NSF- 0919331), the

**Table 4**  
Mean annual carbon fluxes ( $\text{Pg C yr}^{-1}$ ) for the 2000s and 2090s estimated with LPJ and LPJ-STM.

	LPJ						LPJ-STM					
	NPP		$R_H$		NEP		NPP		$R_H$		NEP	
	2000s	2090s	2000s	2090s	2000s	2090s	2000s	2090s	2000s	2090s	2000s	2090s
POL_L	16.7	18.3	14.9	16.3	1.8	2.0	17.2	18.8	14.4	16.3	2.8	2.5
POL_M	16.6	18.2	14.8	16.7	1.8	1.5	17.1	18.8	14.4	16.6	2.7	2.2
POL_H	16.8	18.8	14.9	17.3	1.9	1.5	17.4	19.4	14.5	17.4	2.9	2.0
REF_L	16.6	24.4	14.9	24.0	1.7	0.4	17.2	25.2	14.5	24.1	2.7	1.1
REF_M	16.6	25.1	14.7	26.0	1.9	−0.9	17.1	25.9	14.4	26.2	2.7	−0.3
REF_H	16.9	26.9	14.9	31.1	2.0	−4.2	17.4	27.8	14.5	31.4	2.9	−3.6

NSF Carbon and Water in the Earth Program (NSF-0630319), the NASA Land Use and Land Cover Change program (NASA- NNX09AI26G) and Department of Energy (DE-FG02-08ER64599). The computing is supported by Rosen Center of high performance computing at Purdue.

## References

- Abbott, B.W., et al., 2016. Biomass offsets little or none of permafrost carbon release from soils, streams, and wildfire: an expert assessment. *Environ. Res. Lett.* 11, 034014. <http://dx.doi.org/10.1088/1748-9326/11/3/034014>.
- Anisimov, O.A., Reneva, S., 2006. Permafrost and changing climate: the Russian perspective. *Ambio* 35 (4), 169–175.
- Biskaborn, B.K., Lanckman, J.P., Lantuit, H., Elger, K., Dmitry, S., William, C., Vladimir, R., 2015. The new database of the global terrestrial network for permafrost (GTN-P). *Earth System Science Data* 7, 245–259.
- Bockheim, J.G., 2007. Importance of cryoturbation in redistributing organic carbon in permafrost-affected soils. *Soil Sci. Soc. Am. J.* 71, 1335–1342.
- Camill, P., 2005. Permafrost thaw accelerates in boreal peatlands during late-20th century climate warming. *Clim. Chang.* 68, 135–152.
- Campbell, J.S., Norman, J.M., 1998. *An Introduction to Environmental Biophysics* 286 pp. Springer.
- Clarke, L., Edmonds, J., Jacoby, H., Pitcher, H., Reilly, J., Richels, R., 2007. Scenarios of greenhouse gas emissions and atmospheric concentrations. Sub-report 2.1A of Synthesis and Assessment Product 2.1 by the U.S. Climate Change Science Program and the Subcommittee on Global Change Research. Department of Energy, Office of Biological and Environmental Research, Washington, DC, USA (106 pp).
- Euskirchen, S.E., McGuire, A.D., Kicklighter, D.W., Zhuang, Q., Clein, J.S., Dargaville, R.J., Dye, D.G., Kimball, J.S., McDonald, K.C., Melillo, J.M., Romanovsky, V.E., Smith, N.V., 2006. Importance of recent shifts in soil thermal dynamics on growing season length, productivity, and carbon sequestration in terrestrial high-latitude ecosystems. *Glob. Chang. Biol.* 12, 731–750.
- FAO, 1991. *The Digitized Soil Map of the World (Release 1.0)*. 67(1). Food and Agriculture Organization of the United Nations, Rome.
- FAO/IIASA/ISRIC/ISSCAS/JRC, 2012. *Harmonized World Soil Database (version 1.2)*. FAO, Rome, Italy (IIASA, Laxenburg, Austria).
- Forkel, M., Carvalhais, N., Rödenbeck, C., Keeling, R., Heimann, M., Thonicke, K., Zaehe, S., Reichstein, M., 2016. Enhanced seasonal CO<sub>2</sub> exchange caused by amplified plant productivity in northern ecosystems. *Science* 351 (6274), 696–699.
- Gerten, D., Schaphoff, S., Haberlandt, U., Lucht, W., Sitch, S., 2004. Terrestrial vegetation and water balance – hydrological evaluation of a dynamic global vegetation model. *J. Hydrol.* 286, 249–270.
- Grosse, G., et al., 2011. Vulnerability of high-latitude soil organic carbon in North America to disturbance. *J. Geophys. Res.* 116, G00K06. <http://dx.doi.org/10.1029/2010JG001507>.
- Hansson, K., Šimůnek, J., Mizoguchi, M., Lundin, L., van Genuchten, M.Th., 2004. Water flow and heat transport in frozen soil: numerical solution and freeze–thaw applications. *Vadose Zone J.* 3, 693–704.
- Harden, J.W., et al., 2012. Field information links permafrost carbon to physical vulnerabilities of thawing. *Geophys. Res. Lett.* 39, L15704. <http://dx.doi.org/10.1029/2012GL01958>.
- Hartley, I.P., Garnett, M.H., Sommerkorn, M., Hopkins, D.W., Fletcher, B.J., Sloan, V.L., Phoenix, G.K., Wookey, P.A., 2012. A potential loss of carbon associated with greater plant growth in the European Arctic. *Nat. Clim. Chang.* 2, 875–879.
- Hayes, D.J., Kicklighter, D.W., McGuire, A.D., Chen, M., Zhuang, Q., Yuan, F., Melillo, J.M., Wullschlaeger, S.D., 2014. The impacts of recent permafrost thaw on land-atmosphere greenhouse gas exchange. *Environ. Res. Lett.* 9, 045005.
- Heimann, M., et al., 1998. Evaluation of terrestrial carbon cycle models through simulations of the seasonal cycle of atmospheric CO<sub>2</sub>: first results of a model intercomparison study. *Global Biogeochem. Cycles* 12 (1), 1–24.
- Hobara, S., McCalley, C., Koba, K., Giblin, A.E., Weiss, M.S., Gettel, G.M., Shaver, G.R., 2006. Nitrogen fixation in an arctic tundra watershed: a key atmospheric N source. *Arct. Antarct. Alp. Res.* 38, 363–372.
- Hugelius, G., Kuhry, P., Tarnocai, C., Virtanen, T., 2010. Soil organic carbon pools in a periglacial landscape; a case study from the Central Canadian Arctic. *Permafrost Periglac.* 21, 16–29.
- Hugelius, G., Strauss, J., Zubrzycki, S., Harden, J.W., Schuur, E.A.G., Ping, C.-L., Schirmermeister, L., Grosse, G., Michaelson, G.J., Koven, C.D., O'Donnell, J.A., Elberling, B., Mishra, U., Camill, P., Yu, Z., Palmtag, J., Kuhry, P., 2014. Estimated stocks of circumpolar permafrost carbon with quantified uncertainty ranges and identified data gaps. *Biogeosciences* 11, 6573–6593. <http://dx.doi.org/10.5194/bg-11-6573-2014>.
- Ise, T., Dunn, A.L., Wofsy, S.C., Moorcroft, P.R., 2008. High sensitivity of peat decomposition to climate change through water–table feedback. *Nat. Geosci.* 1 (11), 763–766. <http://dx.doi.org/10.1038/ngeo331>.
- Jiang, Y., Zhuang, Q., O'Donnell, J.A., 2012a. Modeling thermal dynamics of active layer soils and near-surface permafrost using a fully coupled water and heat transport model. *J. Geophys. Res.* 117, D11110. <http://dx.doi.org/10.1029/2012JD017512>.
- Jiang, Y., Zhuang, Q., Schaphoff, S., Sitch, S., Sokolov, A., Kicklighter, D., Melillo, J., 2012b. Uncertainty analysis of vegetation distribution in the northern high latitudes during the 21st century with a dynamic vegetation model. *Ecology and Evolution*. <http://dx.doi.org/10.1002/ece3.85>.
- Jiang, Y., Rocha, A.V., O'Donnell, J.A., Drysdale, J.A., Rastetter, E.B., Shaver, G.R., Zhuang, Q., 2015. Contrasting soil thermal responses to fire in Alaskan tundra and boreal forest. *J. Geophys. Res. Earth Surf.* 120, 363–378.
- Jobbagy, E.G., Jackson, R.B., 2000. The vertical distribution of soil organic carbon and its relation to climate and vegetation. *Ecol. Appl.* 10, 423–436.
- Johnston, C.E., Ewing, S.A., Harden, J.W., Varner, R.K., Wickland, K.P., Koch, J.C., Fuller, C.C., Manies, K., Jorgenson, M.T., 2014. Effect of permafrost thaw on CO<sub>2</sub> and CH<sub>4</sub> exchange in a western Alaska peatland chronosequence. *Environ. Res. Lett.* 9, 085004.
- Jorgenson, M.T., Racine, C.H., Walters, J.C., Osterkamp, T.E., 2001. Permafrost degradation and ecological changes associated with a warming climate in Central Alaska. *Clim. Chang.* 48 (4), 551–571.
- Jorgenson, M.T., Shur, Y.L., Pullman, E.R., 2006. Abrupt increase in permafrost degradation in Arctic Alaska. *Geophysical Research Letters* 33, L02503. <http://dx.doi.org/10.1029/2008GL033985>.
- Kaminski, T., Heimann, M., Giering, R., 1999. A coarse grid three-dimensional global inverse model of the atmospheric transport: 2. Inversion of the transport of CO<sub>2</sub> in the 1980s. *J. Geophys. Res.* 105, 18555–18581.
- Kanevskiy, M., Shur, Y., Fortier, D., Jorgenson, M.T., Stephani, E., 2011. Cryostratigraphy of late Pleistocene syngenetic permafrost (yedoma) in northern Alaska, Itkillik River exposure. *Quat. Res.* 75 (3), 584–596.
- Keeling, C., Whorf, T., 2005. *Atmospheric CO<sub>2</sub> Records from Sites in the SIO Air Sampling Network*. Trends: A Compendium of Data on Global Change. Carbon Dioxide Information Analysis Center, Oak Ridge National Laboratory, US Department of Energy, Oak Ridge, TN, USA.
- Keuper, F., van Bodegom, P.M., Dorrepaal, E., Weedon, J.T., van Hal, J., van Logtestijn, R.S.P., Aerts, R., 2012. A frozen feast: thawing permafrost increases plant-available nitrogen in subarctic peatlands. *Glob. Chang. Biol.* 18, 1998–2007.
- Koch, J.C., Kikuchi, C.P., Wickland, K.P., Schuster, P., 2014. Runoff sources and flow paths in a partially burned, upland boreal catchment underlain by permafrost. *Water Resour. Res.* 50, 8141–8158.
- Koch, J.C., Runkel, R.L., Striegl, R., McKnight, D.M., 2013. Hydrologic controls on the transport and cycling of carbon and nitrogen in a boreal catchment underlain by continuous permafrost. *J. Geophys. Res. Biogeosci.* 118, 698–712.
- Koven, C.D., 2013. Boreal carbon loss due to poleward shift in low-carbon ecosystems. *Nat. Geosci.* 6, 452–456.
- Koven, C.D., Ringeval, B., Friedlingstein, P., Ciais, P., Cadule, P., Khvorostyanov, D., Krinner, G., Tarnocai, C., 2011. Permafrost carbon–climate feedbacks accelerate global warming. *P. Natl. Acad. Sci.* 108, 14769–14774. <http://dx.doi.org/10.1073/pnas.1103910108>.
- Lawrence, D.M., Slater, A.G., Swenson, S.C., 2012. Simulation of present-day and future permafrost and seasonally frozen ground conditions in CCSM4. *J. Clim.* 25, 2207–2225.
- MacDougall, A.H., Avis, C.A., Weaver, A.J., 2012. Significant contribution to climate warming from the permafrost carbon feedback. *Nat. Geosci.* <http://dx.doi.org/10.1038/ngeo1573>.
- Mack, M.C., Schuur, E.A.G., Bret-Harte, M.S., Shaver, G.R., Chapin, F.S., 2004. Ecosystem carbon storage in arctic tundra reduced by long-term nutrient fertilization. *Nature* 431, 440–443.
- Mishra, U., Jastrow, J.D., Matamala, R., Hugelius, G., Koven, C.D., Harden, J.W., Ping, C.L., Michaelson, G.J., Fan, Z., Miller, R.M., McGuire, A.D., 2013. Empirical estimates to reduce modeling uncertainties of soil organic carbon in permafrost regions: a review of recent progress and remaining challenges. *Environ. Res. Lett.* 8 (3), 035020.
- Mitchell, T., Jones, P., 2005. An improved method of constructing a database of monthly climate observations and associated high-resolution grids. *Int. J. Climatol.* 25, 693–712.
- Nordin, A., Schmidt, I.K., Shaver, G.R., 2004. Nitrogen uptake by arctic soil microbes and plants in relation to soil nitrogen supply. *Ecology* 85, 955–962.
- O'Donnell, J.A., Harden, J.W., McGuire, A.D., Kanevskiy, M.Z., Jorgenson, M.T., Xu, X., 2011. The effect of fire and permafrost interactions on soil carbon accumulation in an upland black spruce ecosystem of interior Alaska: implications for post-thaw carbon loss. *Glob. Chang. Biol.* 17, 1461–1474.
- Oechel, W.C., Vourlitis, G.L., Hastings, S.J., Ault, R.P., Bryant, P., 1998. The effects of water table manipulation and elevated temperature on the net CO<sub>2</sub> flux of wet sedge tundra ecosystems. *Glob. Chang. Biol.* 4, 77–90.
- Olefeldt, D., Roulet, N.T., Bergeron, O., Crill, P., Bäckstrand, K., Christensen, T.R., 2012. Net carbon accumulation of a high-latitude permafrost palsamire similar to permafrost-free peatlands. *Geophys. Res. Lett.* 39, L03501. <http://dx.doi.org/10.1029/2011GL050355>.
- Olivas, P.C., Oberbauer, S.F., Tweedie, C.E., Oechel, W.C., Kuchy, A., 2010. Responses of CO<sub>2</sub> flux components of Alaskan Coastal Plain tundra to shifts in water table. *J. Geophys. Res.* 115, G00I05. <http://dx.doi.org/10.1029/2009JG001254>.
- Osterkamp, T.E., 2007. Characteristics of the recent warming of permafrost in Alaska. *Journal of Geophysical Research–Earth Surface* 112, F02S02. <http://dx.doi.org/10.1029/2006JF000578>.
- Osterkamp, T.E., Vierek, L., Shur, Y., Jorgenson, M.T., Racine, C., Doyle, A., Boone, R.D., 2000. Observations of thermokarst and its impact on boreal forests in Alaska, U.S.A. *Arctic Antarctic and Alpine Research* 32, 303–315.
- Rocha, A.V., Loranty, M.M., Higuera, P.E., Mack, M.C., Hu, F.S., Jones, B.M., Breen, A.L., Rastetter, E.B., Goetz, S.J., Shaver, G.R., 2012. The footprint of Alaskan tundra fires during the past half-century: implications for surface properties and radiative forcing. *Environ. Res. Lett.* 7, 044039.
- Romanovsky, V.E., Osterkamp, T.E., 2000. Effects of unfrozen water on heat and mass transport processes in the active layer and permafrost. *Permafrost Periglac.* 11, 219–239.
- Romanovsky, V.E., Smith, S.L., Christiansen, H.H., Shiklomanov, N.I., Streletskiy, D.A., Drozdov, D.S., Malkova, G.V., Oberman, N.G., Kholodov, A.L., Marchenko, S.S., 2015. Terrestrial permafrost [in “state of the climate in 2014”]. *Bull. Amer. Meteor. Soc.* 96 (7), S139–S141.
- Saito, H., Šimůnek, J., Mohanty, B.P., 2006. Numerical analysis of coupled water, vapor, and heat transport in the vadose zone. *Vadose Zone J.* 5, 784–800.

- Schaphoff, S., Heyder, U., Ostberg, S., Gerten, D., Heinke, J., Lucht, W., 2013. Contribution of permafrost soils to the global carbon budget. *Environ. Res. Lett.* 8, 014026.
- Schirmer, L., Grosse, G., Wetterich, S., Overduin, P.P., Strauss, J., Schuur, E.A.G., Hubberten, H.-W., 2011. Fossil organic matter characteristics in permafrost deposits of the northeast Siberian Arctic. *J. Geophys. Res.* 116, G00M02. <http://dx.doi.org/10.1029/2011JG001647>.
- Schneider von Deimling, T., Meinshausen, M., Levermann, A., Huber, V., Frieler, K., Lawrence, D.M., Brovkin, V., 2012. Estimating the near-surface permafrost-carbon feedback on global warming. *Biogeosciences* 9, 649–665. <http://dx.doi.org/10.5194/bg-9-649-2012>.
- Schuur, E.A.G., Abbott, B.W., Bowden, W.B., et al., 2013. Expert assessment of vulnerability of permafrost carbon to climate change. *Clim. Chang.* 119, 359–374.
- Schuur, E.A.G., Crummer, K.G., Vogel, J.G., Mack, M.C., 2007. Plant species composition and productivity following permafrost thaw and thermokarst in Alaskan tundra. *Ecosystems* 10, 208–292.
- Shaver, G.R., Bret-Harte, S.M., Jones, M.H., Johnstone, J., Gough, L., Laundre, J., Chapin, F.S., 2001. Species composition interacts with fertilizer to control long-term change in tundra productivity. *Ecology* 82, 3163–3181.
- Shur, Y., French, H.M., Bray, M., Anderson, D., 2004. Syngenetic permafrost growth: cryostratigraphic observations from the CRREL tunnel, Fairbanks, Alaska. *Permafrost. Periglac. Process.* 15, 339–347.
- Sitch, S., Smith, B., Prentice, I.C., Arneth, A., Bondeau, A., Cramer, W., Kaplan, J.O., Levis, S., Lucht, W., Sykes, M.T., Thonicke, K., Venevsky, S., 2003. Evaluation of ecosystem dynamics, plant geography and terrestrial carbon cycling in the LPJ dynamic global vegetation model. *Glob. Change Biol.* 14, 2015–2039.
- Sitch, S., et al., 2008. Evaluation of the terrestrial carbon cycle, future plant geography and climate-carbon cycle feedbacks using five dynamic global vegetation models (DGVMs). *Glob. Change Biol.* 14, 2015–2039.
- Slater, A.G., Lawrence, D.M., 2013. Diagnosing present and future permafrost from climate models. *J. Clim.* 26 (15), 5608–5623.
- Smith, B., Warlind, D., Arneth, A., Hickler, T., Leadley, P., Siltberg, J., Zaehle, S., 2014. Implications of incorporating N cycling and N limitations on primary production in an individual-based dynamic vegetation model. *Biogeosciences* 11, 2027–2054.
- Sokolov, A.P., Kicklighter, D.W., Melillo, J.M., Felzer, B.S., Schlosser, C.A., Cronin, T.W., 2008. Consequences of considering carbon-nitrogen interactions on the feedbacks between climate and the terrestrial carbon cycle. *J. Clim.* 21, 3776–3796.
- Sokolov, A.P., Schlosser, C.A., Dutkiewicz, S., Paltsev, S., Kicklighter, D.W., Jacoby, H.D., Prinn, R.G., Forest, C.E., Reilly, J., Wang, C., Felzer, B., Sarofim, M.C., Scott, J., Stone, P.H., Melillo, J.M., Cohen, J., 2005. The MIT Integrated Global System Model (IGSM) Version 2: Model Description and Baseline Evaluation. MIT Joint Program on the Science and Policy of Global Change, Cambridge, Massachusetts Report 124.
- Sokolov, A.P., Stone, P.H., Forest, C.E., Prinn, R.G., Sarofim, M.C., Webster, M., Paltsev, S., Schlosser, C.A., Kicklighter, D.W., Dutkiewicz, S., Reilly, J., Wang, C., Felzer, B., Jacoby, H.D., 2009. Probabilistic forecast for 21st century climate based on uncertainties in emissions (without policy) and climate parameters. *J. Clim.* 22 (19), 5175–5204.
- Stendel, M., Christensen, J.H., 2002. Impact of global warming on permafrost conditions in a coupled GCM. *Geophysical Research Letters* 29 (13), 1632. <http://dx.doi.org/10.1029/2007GL031002>.
- Streletskiy, D.A., Sherstiukov, A.B., Frauenfeld, O.W., Nelson, F.E., 2015. Changes in the 1963–2013 shallow ground thermal regime in Russian permafrost regions. *Environmental Research Letters* 10 (12), 125005.
- Sulman, B.N., Desai, A.R., Cook, B.D., Saliendra, N.Z., Mackay, D.S., 2009. Contrasting carbon dioxide fluxes between a drying shrub wetland in Northern Wisconsin, USA, and nearby forests. *Biogeosciences* 6, 1115–1126.
- Sulman, B.N., Desai, A.R., Saliendra, N.Z., Lafleur, P.M., Flanagan, L.B., Sonntag, O., Mackay, D.S., Barr, A.G., van der Kamp, G., 2010. CO<sub>2</sub> fluxes at northern fens and bogs have opposite responses to inter-annual fluctuations in water table. *Geophys. Res. Lett.* 37 (19), L19702. <http://dx.doi.org/10.1029/2010GL044018>.
- Tarnocai, C., Canadell, J.G., Schuur, E.A.G., Kuhry, P., Mazhitova, G., Zimov, S., 2009. Soil organic carbon pools in the northern circumpolar permafrost region. *Glob. Biogeochem. Cycles* 23 (2).
- Tchebakova, N.M., Parfenova, E., Soja, A.J., 2009. The effects of climate, permafrost and fire on vegetation change in Siberia in a changing climate. *Environ. Res. Lett.* 4 (4), 045013.
- Todd-Brown, K.E.O., Randerson, J.T., Post, W.M., Hoffman, F.M., Tarnocai, C., Schuur, E.A.G., Allison, S.D., 2013. Causes of variation in soil carbon simulations from CMIP5 Earth system models and comparison with observations. *Biogeosciences* 10, 1717–1736.
- Treat, C.C., Jones, M.C., Camill, P., Gallego-Sala, A., Garneau, M., Harden, J.W., Hugelius, G., Klein, E.S., Kokfelt, U., Kuhry, P., et al., 2016. Effects of permafrost aggradation on peat properties as determined from a pan-Arctic synthesis of plant macrofossils. *J. Geophys. Res. Biogeosci.* 121, 78–94.
- Turetsky, M.R., et al., 2010. Recent acceleration of biomass burning and carbon losses in Alaskan forests and peatlands. *Nat. Geosci.* 4, 27–31.
- Walter-Anthony, K.M., Zimov, S.A., Grosse, G., Jones, M.C., Anthony, P.M., Chapin, F.S., Finlay, J.C., Mack, M.C., Davydov, S., Frenzel, P., Frolking, S., 2014. A shift of thermokarst lakes from carbon sources to sinks during the Holocene epoch. *Nature* 511, 452–456.
- Wania, R., Ross, I., Prentice, I.C., 2009a. Integrating peatlands and permafrost into a dynamic global vegetation model: 2. Evaluation and sensitivity of vegetation and carbon cycle processes. *Global Biogeochem. Cycles* 23, GB3015. <http://dx.doi.org/10.1029/2008GB003413>.
- Wania, R., Ross, I., Prentice, I.C., 2009b. Integrating peatlands and permafrost into a dynamic global vegetation model: 1. Evaluation and sensitivity of physical land surface processes. *Global Biogeochem. Cycles* 23, GB3014. <http://dx.doi.org/10.1029/2008GB003412>.
- Webster, M., Sokolov, A.P., Reilly, J., Forest, C.E., Paltsev, S., Schlosser, C.A., Wang, C., Kicklighter, D.W., Sarofim, M., Melillo, J.M., Prinn, R.G., Jacoby, H.D., 2012. Analysis of climate policy targets under uncertainty. *Clim. Chang.* 112, 569–583.
- Xu, R., Prentice, I.C., 2008. Terrestrial nitrogen cycle simulation with a dynamic global vegetation model. *Glob. Change Biol.* 14, 1745–1764.
- Yoshikawa, K., Hinzman, L.D., 2003. Shrinking thermokarst ponds and groundwater dynamics in discontinuous permafrost near council, Alaska. *Permafrost. Periglac. Process.* 14 (2), 151–160.
- Yu, Z.C., Loisel, J., Brosseau, D.P., Beilman, D.W., Hunt, S.J., 2010. Global peatland dynamics since the last glacial maximum. *Geophys. Res. Lett.* 37, L13402. <http://dx.doi.org/10.1029/2010GL043584>.
- Zhang, Y., Chen, W.J., Riseborough, D.W., 2008. Transient projections of permafrost distribution in Canada during the 21st century under scenarios of climate change. *Glob. Planet. Chang.* 60 (3–4), 443–456.
- Zobler, L., 1986. A World Soil File for Global Climate Modeling. National Aeronautics and Space Administration, Goddard Space Flight Center, Institute for Space Studies, NASA Technical Memorandum. 87802 (32 pp).